Modelling Activation and Connectivity in the Brain: An fMRI Study during Externally Triggered Finger Tapping Task

Ahmad Nazlim Yusoff and Khairiah Abdul Hamid

Diagnostic Imaging and Radiotherapy Program,
School of Diagnostic and Applied Health Sciences,
Faculty of Health Sciences, Universiti Kebangsaan Malaysia,
Jalan Raja Muda Abdul Aziz, 50300 Kuala Lumpur, Malaysia

E-mail: nazlim@fskb.ukm.my

ABSTRACT

Brain activation within and effective connectivity between two significantly activated left and right primary motor regions ($M1_{left}$ and $M1_{right}$) were modelled using functional magnetic resonance imaging datasets of seven subjects obtained from an externally triggered unilateral and bilateral finger tapping experiment. Unilateral tapping exhibited contra lateral activation while bilateral tapping activated both the $M1_{left}$ and $M1_{right}$ regions. Unlike bilateral tapping that exhibited a relatively equal change of $M1_{left}$ and $M1_{right}$ signal at the coordinates of maximum intensity, the value is significantly lower in $M1_{left}$ as compared to $M1_{right}$ for unilateral tapping. The effective connectivity between $M1_{left}$ and $M1_{right}$ during bilateral tapping of hand fingers can be explained by a bilinear causal model, which is averagely preferred by five subjects (Dirichlet parameter estimate, $\alpha_d \approx 5$). The regional connectivities are however not gated (influenced) by any of the two M1s, ruling out the possibility of the non-linear behavior of connections between both M1s. This study has been able to fit the effective connectivity between $M1_{left}$ and $M1_{right}$ with a bilinear model that has the lowest free energy (F) of -644.70 and the largest likelihood (4.77×10^{39}), posterior ($\varphi = 1.00$), expected ($r = 0.67$) and exceedance ($\psi = 0.92$) probabilities.

Keywords: Dynamic causal modeling, Bayesian model selection, bilinear model, expected probability, exceedance probability.

1. INTRODUCTION

Human brain can be thought of as a control center in a human body. It acts as an instruction hub for various kinds of mechanism in the body. Instructions are conveyed through the transmission of synaptic signal which is governed by the brain structure-function relationship (Nolte (2009)). The relationship between the brain structure and function can be modeled. Modeling involves investigating the underlying relationships between the

conceptual, anatomical, statistical and causal nature of the brain and its responses (Friston (2005)).

Modelling the structure-function relationship pertains to first, identifying the areas that constitute a neuronal system and second the construction of physiologically and physically plausible models constituting these areas (Friston *et al.* (2003)). The parameter of interest is known as the effective connectivity which is defined as the influence that the elements of a neuronal system exert over another (Friston *et al.* (2003)). The third step in modeling is model estimation in which the neuronal parameters constituting a model are estimated. Finally, the models are compared to test the null hypothesis that no single model is better than any other competing models (Stephan *et al.* (2009, 2010)). The dynamic causal modeling (DCM) was implemented in model construction, estimation and comparison in this study. A detailed explanation of the underlying mathematical and biophysical concepts can be found elsewhere (Friston *et al.* (2003)).

DCM treats the brain as a dynamic input-state-output system. It is basically a nonlinear system identification procedure and uses Bayesian (Stephan *et al.* (2009)) parameter estimation to draw inferences about the effective connectivity between different regions in the brain. The Dynamic Causal Models (DCMs) that are constructed using neuroimaging time series data such as fMRI explain the interaction among neuronal populations at a cortical level. The change of neuronal state vector (x) in time (dx/dt) can be summarized in matrix form as bilinear differential equation (Friston *et al.* (2003)). Three sets of parameter are estimated for bilinear causal models, which are (1) the intrinsic connection strength between regions in the absence of any external experimental input, (2) the modulatory input that changes the intrinsic connection strength induced by experimental input and (3) the direct influence of a stimulus on a given region.

This paper is about analyzing the spatial and height extent of activation and modelling the effective connectivity between spatially activated primary motor areas ($M1_{left}$ and $M1_{right}$) in the brain using Statistical Parametric Mapping (SPM) and DCM on Functional Magnetic Resonance Imaging (fMRI) data. To date, SPM and DCM have been widely used in cognitive neuroscience to investigate various aspects of functional specialization and effective connectivity in the human brain (Grefkes *et al.* (2008); Ahmad Nazlim Yusoff *et al.* (2010a); Aini Ismafairus Abd Hamid *et al.* (2011); Ahmad Nazlim Yusoff *et al.* (2010b); Ahmad Nazlim Yusoff *et al.* (2011)).

2. METHODS

2.1 Subject

fMRI examinations were performed on 7 right-handed Malay subjects (two males and five females). The subjects were given informed consent and screening forms as required by the Institutional Ethics Committee (IEC). The subjects were interviewed on their health condition prior to the scanning session. Prior to the fMRI scans, the subjects' handedness was tested using the Edinburgh Handedness Inventory (Oldfield (1971)). The subjects were also told not to move their head during the scan. Head movement will also cause artifacts on functional images due to the voxels that are not correctly registered (or moving) during the scan resulting in significant changes in signal intensity of that particular voxels over time. The immobilising devices were used together with the head coil in order to minimise head movement.

2.2 fMRI Scans

fMRI examinations were conducted using a 1.5-tesla Magnetic Resonance Imaging (MRI) system (Siemens Magnetom Vision VB33G) equipped with functional imaging option, Echo Planar Imaging (EPI) capabilities and a Radiofrequency (RF) head coil used for signal transmission and reception. Gradient Echo - Echo Planar Imaging (GRE-EPI) pulse sequence with the following parameters were applied: Repetition Time (TR) = 5 s, Acquisition Time (TA) = 3 s, Echo Time (TE) = 66 ms, Field of View (FOV) = 210×210 mm, flip angle = $90°$, matrix size = 128×128 and slice thickness = 4 mm.

Using the midsagittal scout images (TR = 15 ms, TE = 6 ms, FOV = 300×300 mm, flip angle = $30°$, matrix size = 128×128 and magnetic field gradient = 15 mT/m) produced earlier, 35 axial slice positions (1 mm interslice gap) were oriented in the anterior-posterior commissure (AC-PC) plane. This covers the whole brain volume. In addition, high resolution anatomical images of the entire brain were obtained using a strongly T1-weighted spin echo pulse sequence with the following parameters: TR = 1000 ms, TE = 30 ms, FOV = 210×210 mm, flip angle = $90°$, matrix size = 128×128 and slice thickness = 4 mm.

2.3 Experimental paradigm

The subjects were instructed on how to perform the motor activation task and were allowed to practice prior to the scanning. The subjects had to tap all four fingers against the thumb beginning with the thumb-index finger contact and proceeding to the other fingers in sequence which would then begin anew with contact between thumb and index finger. This study used an externally triggered finger tapping task. The tapping of the fingers were triggered by the ticking sound produced by a signal generator that was connected to the speaker. The ticking sound was transmitted to the subject through an air-filled tube and the headphone via an intercom. The tapping rate was two times in one second (2 Hz), using an intermediate force between too soft and too hard.

A six-cycle active-rest paradigm which was alternately and auditorily cued between active and rest was used with each cycle consisted of 10 series of measurements during active state and 10 series of mesurements during resting state. The tapping of the fingers were done unilaterally (UNI_{left} or UNI_{right}) or bilaterally (BIL) in an alternate fashion. The tapping pace between the left and right hand fingers were kept in-phased. Each functional measurement produces 20 axial slices in 3 s (one image slice in 150 ms) with an inter-measurement interval of 2 s. The measurement started with active state. The imaging time for the whole functional scans was 600 s (10 minutes) which produced $120 \times 20 = 2400$ images in total. A high resolution T2*-weighted images were obtained using the voxel size of 1.64 mm $\times$ 1.64 mm $\times$ 4.00 mm.

2.4 Post-processing of data

The MRI data were analysed using MATLAB 7.4 – R2008a (Mathworks Inc. MA, USA) and Statistical Parametric Mapping (SPM8) programming software. A conventional analysis based on the general linear model was used to generate brain activation in the regions of interest using the *T*-statistic for each voxel. Individual subject analysis was performed at corrected significant level (α) of 0.05. For group analysis, the fixed effects analysis (FFX) was used and statistical inferences were also made at significant level (α) of 0.05, corrected for multiple comparisons (Friston *et al.* (1996)).

The relative response change at the coordinates of maximum intensity for the right and left primary motor areas ($M1_{left}$ and $M1_{right}$) for all the tapping conditions was investigated using Statistical Packages for Social Sciences (SPSS) software version 17.0. The relative response change

obtained from SPM analyses for $M1_{left}$ and $M1_{right}$ were compared by means of independent t-test, i.e. the relative response change for $M1_{left}$ (due to right hand tapping) vs. the relative response change for $M1_{right}$ (due to left hand tapping) and the relative response change for $M1_{left}$ vs. the relative response change for $M1_{right}$ during bilateral tapping. The relationship between the relative response change at the coordinates of maximum intensity for $M1_{left}$ and $M1_{right}$ for bilateral tapping was also investigated by means of simple linear regression analysis to determine the existence of any temporal relationship between the two activated areas across all subjects. The normality of the residuals as well as the linearity and homocedascity (equal variance) between the predicted values and the residuals are clarified prior to regression analysis. The independent t and regression analyses considered only the data that are obtained from fMRI measurements during active state. All the results are reported based on significant level (α) of 0.05 with 95% Confidence Interval (CI).

2.5 Dynamic Causal Modeling (DCM)

The effective connectivity among the activated Regions of Interest (ROIs) during bilateral tapping was approached using Dynamic Causal Modeling (DCM10). The two brain regions each of which has a central role in motor control were considered. The ROIs are $M1_{left}$ and $M1_{right}$. The anatomical location of the activation peak for these two regions having significant voxels ($p_{corrected} < 0.05$) was confirmed using the Anatomy Toolbox (Eickoff et $al.$ (2005)). These two ROIs for each individual were co-registered with the activation peak obtained from the group analysis of fixed effects (FFX). The peak coordinates for each ROI (defined as a sphere of 4 mm radius) was predetermined so that its displacement is within the 20-mm radius from the peak activation obtained from the FFX activation map. This 20-mm range was allowed for this study due to the relatively large M1 area in any individual. The individual peak coordinates must also be within the same brain region (Grefkes et $al.$ (2008)) with that of FFX, i.e. The precentral gyrus (PCG). Subjects whose coordinates do not fulfill these two criteria will be excluded from DCM analysis.

Figure 1 shows eight biologically and physically plausible linear (Model 1 and 2), bilinear (Model 3 and 4) and nonlinear (Model 5 – 8) dynamic causal models for bilateral tapping of hand fingers, that are constructed based on the two M1s coordinates of all the subjects that have been found to be significantly activated at $\alpha = 0.05$, corrected for multiple comparisons.

In Model 1, both the $M1_{left}$ and $M1_{right}$ regions are bi-directionally connected. The activity in both regions is assumed to be perturbed only by the stimulus-bound input (U_1) originating from the tapping of bilateral (B) hand fingers, while for Model 2, the perturbation is assumed to be also intrinsically caused by the left (L) and right (R) hand finger tapping. Models 3 and 4 are accordingly similar to Models 1 and 2, except that the between-region connections are assumed to be influenced by the modulatory input (U_2) of the left and right hand tapping of fingers.
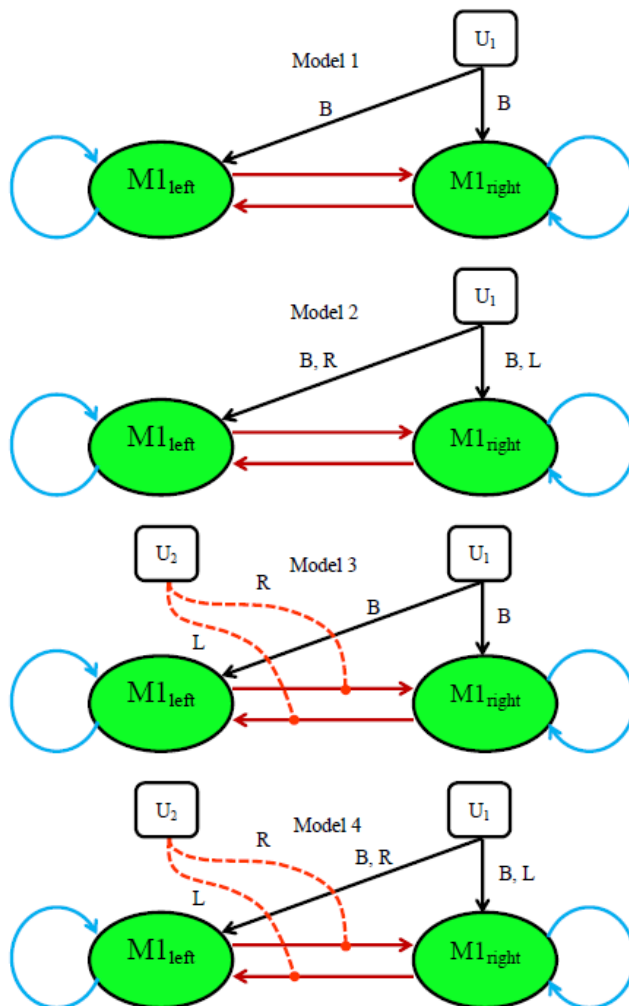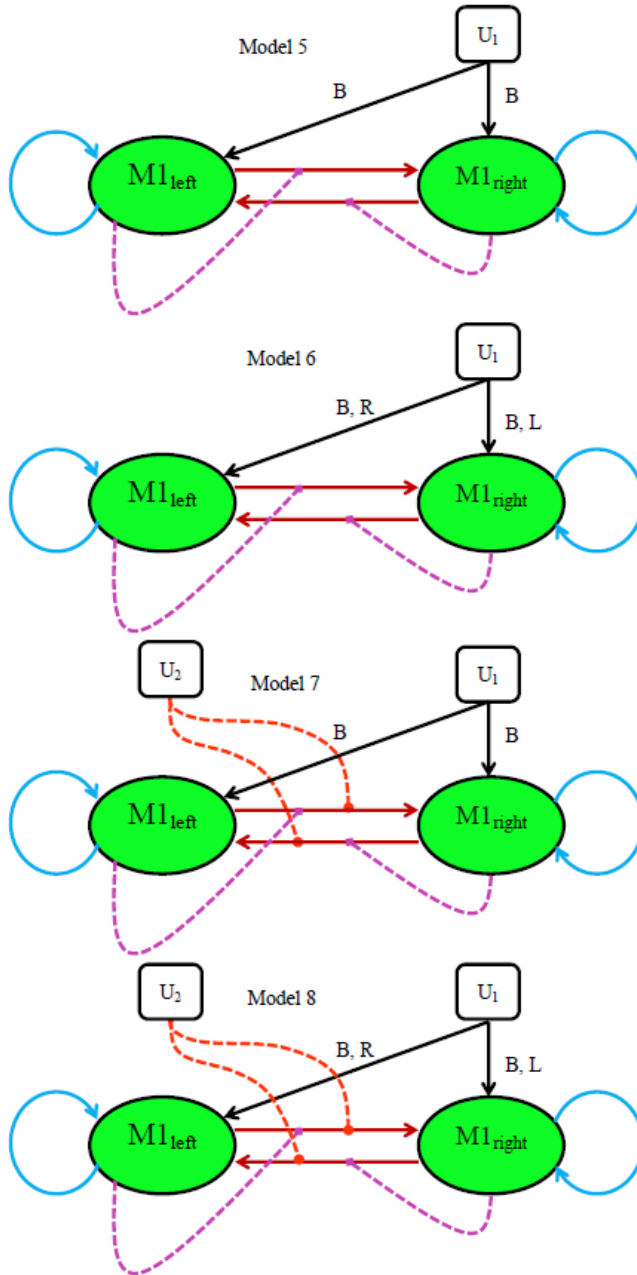
Figure 1: Linear (Models 1 and 2), bilinear (Models 2 and 4) and nonlinear (Model 5 to 8) models constructed based on the two (M1$_{left}$ and M1$_{right}$) regions

The attentional control on the movement of the left and right hand fingers that triggers simultaneously during the externally-triggered bilateral tapping of hand fingers are thought to be the potential sources of U_2. Models 5 – 8 are similar to Model 1 – 4 except that in addition to the stimulus-bound perturbation on regions and modulatory input on connections, the connectivity between the two $M1_{left}$ and $M1_{right}$ regions are also gated by the activity in the region itself. All models are assumed to have self connection on each M1 region. All the models were fitted and inferred over all subjects using DCM10. The models were then compared by means of Bayesian Model Selection (BMS) for group studies (Stephan *et al.* (2009, 2010)) to test the null hypothesis that no single model is better than any other competing models and to obtain a model that has the best balance between fit/accuracy and complexity. All the symbols, lines and arrows used in Figure 1 are explained in Figure 2.
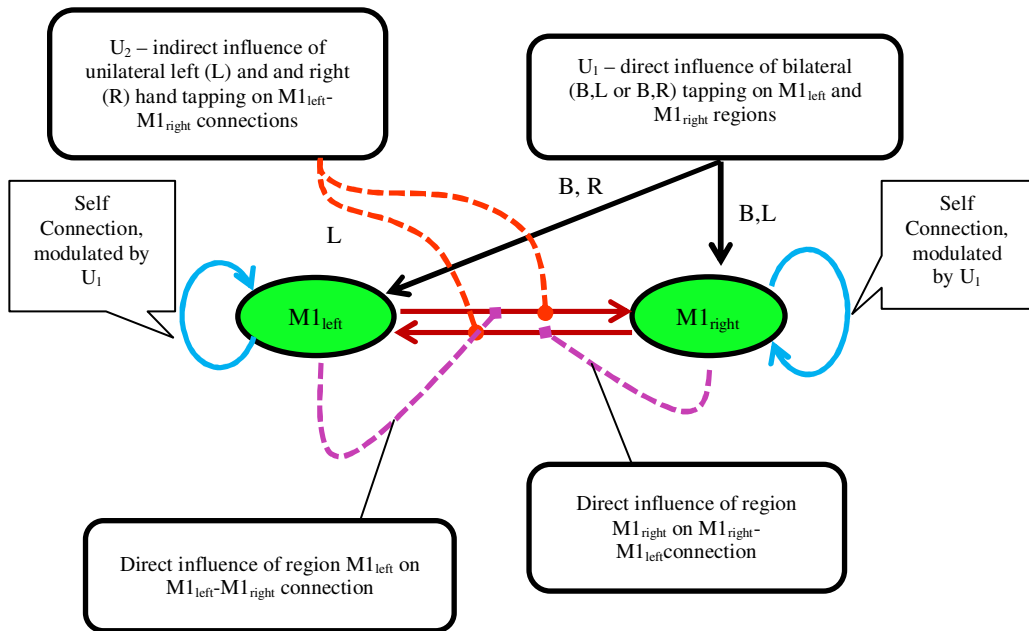

Figure 2: Definition of arrows, lines and symbols used in the dynamic causal models shown in Figure 1. U_1 is the stimulus-bound perturbation while U_2 is the stimulus-free contextual input

3. RESULTS

The subjects' average age and its standard deviation are 24.14 and 2.61 years. All subjects were confirmed to be healthy and right-handed with the average laterality index of 82.14 (in the range of 5th right). Demographical data and a complete handedness test results for all the subjects are depicted in Table 1.

TABLE 1: Demographical data and the results obtained from handedness test using Edinburgh Handedness Inventory for all subjects

Subject	Gender	Age	Race	Laterality index	Decile
S1	Female	25	Malay	85	6th right
S2	Male	21	Malay	80	5th right
S3	Female	26	Malay	70	3rd right
S4	Female	28	Malay	75	4th right
S5	Female	25	Malay	90	7th right
S6	Female	23	Malay	85	6th right
S7	Male	21	Malay	90	7th right

The group FFX results for the pure unilateral and bilateral tapping of hand fingers are shown in Figure 3(a – c). Unilateral left hand finger tapping activated a number of 3939 voxels in the main cluster (peak at 36/-22/48) while unilateral right hand finger tapping indicated a total of 2292 voxels in the main cluster (peak at -38/-12/58). The activated voxels are significant at $p < 0.05$ with $t > 4.68$. The activated areas for unilateral left and right hand finger tapping cover parts of precentral gyrus (PCG), postcentral gyrus (PsCG) and superior frontal gyrus (SFG). Bilateral tapping activated both the $M1_{right}$ and $M1_{left}$ regions with 1892 (peak at 36/-14/66) and 1808 (peak at -38/-12/60) activated voxels ($t > 4.68$, $p < 0.05$) respectively. The area of activation also covers the right and left PCG, PsCG and SFG.

The activation area shown in Figure 3(d) (peak at -36/-24/62, $t > 4.68$, $p < 0.05$) is the conjunction of the effects of the right unilateral tapping with the effects of bilateral tapping minus the left unilateral tapping. It is the area in the brain that specifically controls the tapping of the right hand fingers during both unilateral right and bilateral tapping. The area has been confirmed to be the $M1_{left}$ which covers parts of PCG, PsCG and SFG.

There is only one activation cluster containing 1313 voxels from which 52.0% is in the left Brodmann Area (BA) 6 (15.9% activated), 14.7% is in the left BA1 (21.0% activated), 11.8% is in the left BA4a (13.3% activated) and 5.5% is in the left BA 4p (12.7% activated).

Similarly, Figure 3(e) indicates the area in the brain responsible for controlling the tapping of the left hand fingers during both the unilateral left and bilateral tapping. The activated area is the $M1_{right}$ covering parts of PCG and SFG. The activation area shown (peak at 42/-18/56, $t > 4.68$, $p < 0.05$) was the conjunction of the effects of the left unilateral tapping with the effects of bilateral tapping minus the right unilateral tapping. The activation cluster contains 743 voxels from which 54.4% of cluster is in the right BA6 (9.5% activated), 11.9% of cluster is in the right BA4a (8.0% activated), 6.9% of cluster is in the right BA1 (6.2% activated) and 6.8% of cluster is in the right BA3b (5.5% activated).
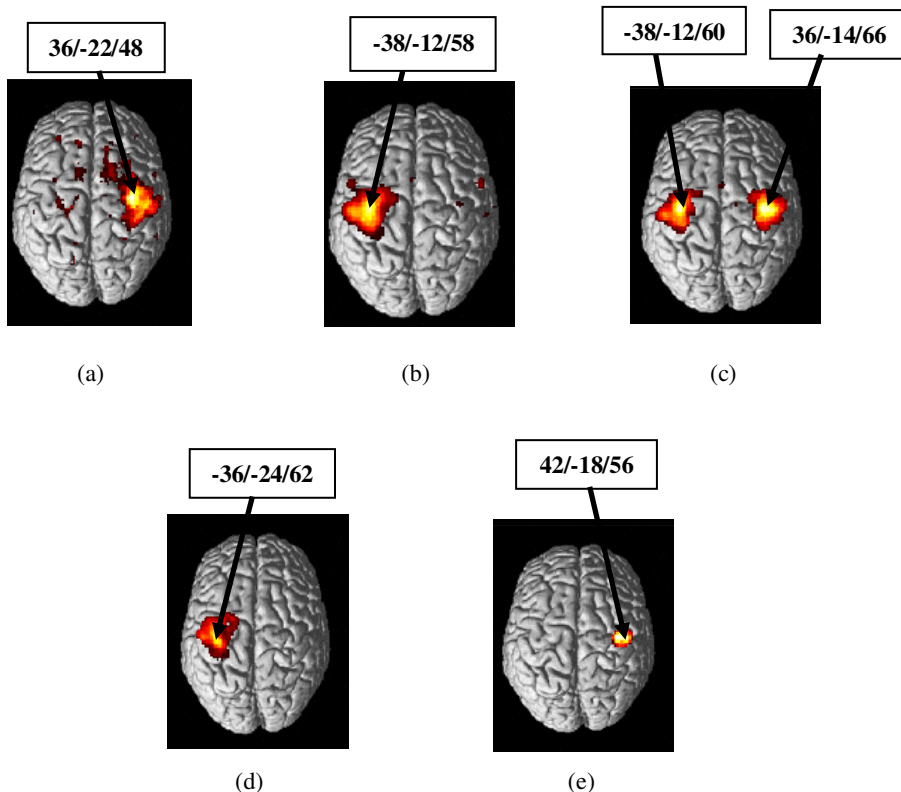

(a)   (b)   (c)

(d)   (e)

Figure 3: Brain activation as explained in the text. The coordinates of maximum intensity are shown in the text box

Figure 4 shows the plots of the relative change of response for $M1_{left}$ and $M1_{right}$ calculated at the respective coordinates of maximum intensity. The locations of the respective coordinate shown on the vertical axes are indicated in Figure 3 (a – c).
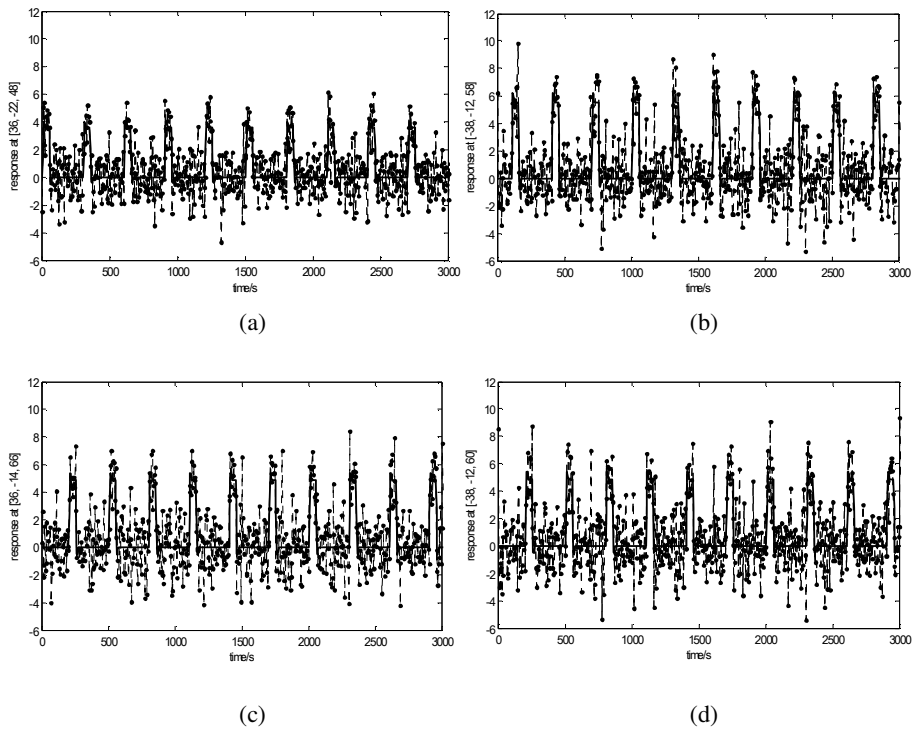

(a)

(b)

(c)

(d)

Figure 4: The relative change in response for all subjects at the point of maximum intensity for (a) $M1_{right}$ (due to unilateral left hand finger tapping), (b) $M1_{left}$ (due to unilateral right hand finger tapping), while (c) and (d) are for $M1_{right}$ and $M1_{left}$ respectively during bilateral tapping of hand fingers. Solid line represents the fitted response while the response plus the error is represented by the solid circles and dashed line. Horizontal axes represent concatenated time points

It can be clearly seen that the relative change in response is relatively lower in $M1_{right}$ (due to the unilateral tapping of the left hand fingers) as compared to in $M1_{left}$ (due to the unilateral tapping of the right hand fingers). Independent t-test indicated that the mean and standard deviation values are 3.15 ± 0.16 and 4.84 ± 0.20 respectively.

The difference has been found to be significant [$n = 140$; $p < 0.001$; 95% CI (-2.12,-1.17)]. However, the change in response is about the same in the $M1_{left}$ and $M1_{right}$ during bilateral tapping from which the values are 4.44 ± 0.18 and 4.36 ± 0.19 respectively and the difference has been found to be insignificant [$n = 140$; $p = 0.77$; 95% CI (-0.43, 0.58)].

The results obtained from regression analysis are depicted in Fig. 5 with (a) the relative response for $M1_{right}$ and $M1_{left}$ as dependent and independent variables respectively and (b) vice versa. In both cases, the predicted and residual data were found to meet the normality, linearity and homocedasticity assumptions. For (a), it can be seen that there exist a positive, linear and significant relationship between the relative response measured at the points of maximum intensity in $M1_{left}$ and $M1_{right}$ regions. The strength of the relationship is good [$n = 140$, $r = 0.73$; $p < 0.001$; 95% CI for $b = 0.57, 0.79$]. Analysis performed in the other direction i.e. the relative response in $M1_{left}$ as dependent variable and the relative response in $M1_{right}$ as independent variable as shown in (b), reveals a slightly different result [$n = 140$; $p < 0.001$; 95% CI for $b = 0.65, 0.90$] but with similar strength of relationship ($r = 0.73$).
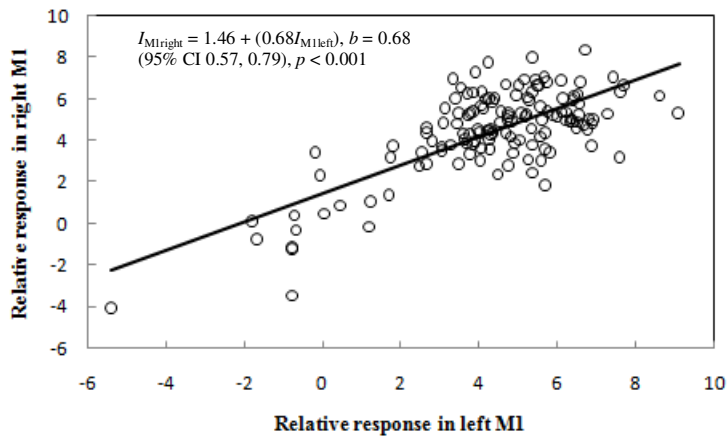
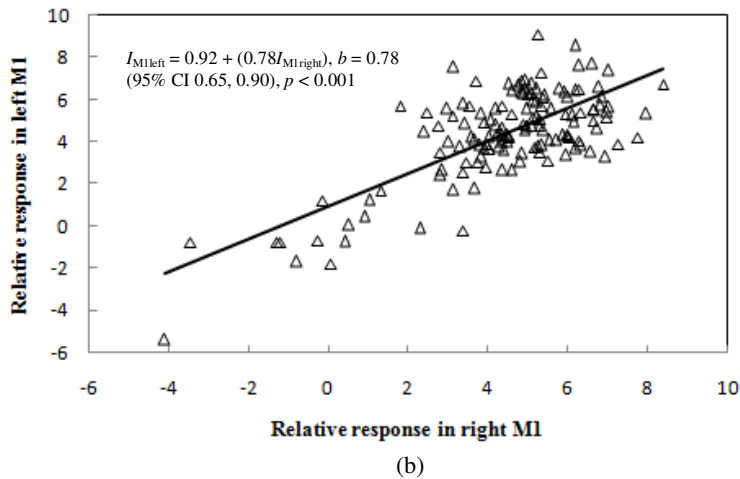$I_{M1right} = 1.46 + (0.68 I_{M1left})$, $b = 0.68$
(95% CI 0.57, 0.79), $p < 0.001$

(a)

(b)

Figure 5: Relationship between the relative response (I) in $M1_{left}$ and $M1_{right}$

Table 2 shows the coordinates of the point of maximum intensity for $M1_{left}$ and $M1_{right}$ obtained from individual subject during bilateral tapping. Also shown for comparison are the coordinates obtained from group FFX for bilateral tapping and conjunction analysis (see also Figure 3 (a – e)). The displacement between the individual subject's coordinates of maximum intensity of $M1_{left}$ and $M1_{right}$ and the coordinates of maximum intensity of $M1_{left}$ and $M1_{right}$ obtained from group FFX for bilateral tapping (d_b) and conjunction analysis (d_c) are also tabulated. It was found that the location of the maximum intensity coordinates for $M1_{left}$ and $M1_{right}$ for all subjects are not greater than 16 mm (2 × the width of the smoothing kernel) from the coordinates obtained from group FFX for bilateral tapping and conjunction analysis, except for Subject 2 from which d_b has been found to be 17.21 mm, but still within the 20-mm distance constrain. The d_b and d_c values for Subject 4 cannot be determined due to the absence of activated voxels in $M1_{left}$ at corrected significant level. This subject was excluded from dynamic causal modelling. Another subject that was excluded from DCM analyses was Subject 6. Even though this subject has indicated significant activation in $M1_{left}$ and $M1_{right}$ regions, the data would not be fitted for Bayesian model averaging (BMA) analysis due to different sequence of trials performed by this subject during the fMRI experiment i.e. [Right, Left, Bilateral] sequence as opposed to the rest of the subjects that use [Left, Right, Bilateral] sequence. The individual subject coordinates shown in Table 2 are the base coordinates for the dynamic causal models shown in Figure 1.

TABLE 2: Individual coordinates of maximum intensity in $M1_{left}$ and $M1_{right}$ during bilateral tapping and their displacement from the coordinates obtained from group FFX and conjunction analyses (also shown at the bottom of the table)

	$M1_{left}$ coordinates	d_b/mm	d_c/mm	$M1_{right}$ coordinates	d_b/mm	d_c/mm
Subject 1	-40/-10/56	4.90	15.75	40/-8/60	9.38	10.95
Subject 2	-38/-24/60	12.00	2.83	38/-30/60	17.21	13.27
Subject 3	-38/-14/64	4.47	10.39	36/-16/68	2.83	13.57
Subject 4	-	-	-	38/-18/56	10.95	4.00
Subject 5	-38/-20/54	10.00	9.17	44/-16/56	12.96	2.83
Subject 6	-30/-24/56	14.97	8.49	38/-16/62	4.90	7.48
Subject 7	-40/-10/56	4.90	15.75	40/-8/60	9.38	10.95
FFX Bilateral	-38/-12/60	0	12.33	36/-14/66	0	12.33
Conjunction	-36/-24/62	12.33	0	42/-18/56	12.33	0

d_b: Displacement of individual from group FFX coordinates of maximum intensity when overlaid onto the same space

d_c: Displacement of individual from conjunction coordinates of maximum intensity when overlaid onto the same space

The results obtained from model comparison are shown in Figure 6 for BMS analysis of (a) FFX and (b) RFX (Stephan (2009)). The bar charts on the left represent the results of family comparison. They clearly show the preference of bilinear model family to linear and nonlinear model families. A detail model comparison results is shown by the bar charts on the right. Bayesian model selection (BMS) has chosen Model 4 as the winning model against the other seven models. The numerical results obtained from model comparison are tabulated in Table 3. From RFX analysis, it can be seen that Model 4 has the lowest sum of free energy (ΣF) value but shows the highest Dirichlet parameter estimate (α_d), expected (r) and exceedance probabilities (ψ). In FFX analysis, Model 4 has the highest likelihood and its probability (φ). The fact that Model 4 is the winning model has been agreed upon by RFX and FFX analyses. This indicates that Model 4 is the model that has the best balance between fit/accuracy and complexity. Thus, the null hypothesis that no single model is better than any other model is rejected.

Modelling Activation and Connectivity in the Brain:
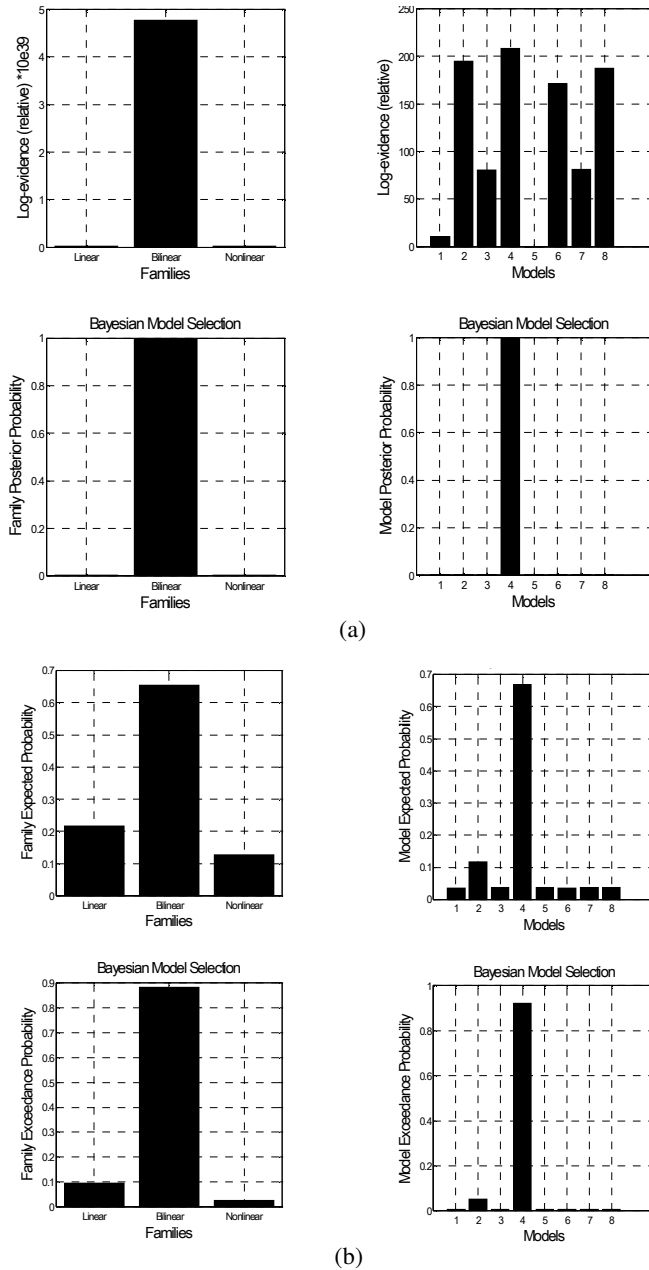An fMRI Study during Externally Triggered Finger Tapping Task

(a)

(b)

Figure 6: Bayesian model selection results for model comparison. Both FFX and RFX
comparison methods prefer Model 4 as the model that has the best
balance between fit/accuracy and complexity

TABLE 3: Data obtained from model comparison using BMS for (a) group random effects analysis (RFX) and (b) group fixed effects analysis (FFX), averaged over 5 subjects

	Model 1	Model 2	Model 3	Model 4	Model 5	Model 6	Model 7	Model 8
Model Type	Linear	Linear	Linear	Linear	Nonlinear	Nonlinear	Nonlinear	Nonlinear
ΣF	-842.7	-657.6	-772.5	-644.7	-852.8	-681.4	-772.0	-664.7
α_d	1.00	1.91	1.00	5.06	1.00	1.01	1.00	1.02
r	0.04	0.12	0.04	0.67	0.04	0.04	0.04	0.04
ψ	0.01	0.05	0.004	0.92	0.01	0.004	0.004	0.01

(a)

	Model 1	Model 2	Model 3	Model 4	Model 5	Model 6	Model 7	Model 8
Model Type	Linear	Linear	Linear	Linear	Nonlinear	Nonlinear	Nonlinear	Nonlinear
ΣF	-842.7	-657.6	-772.5	-644.7	-852.8	-681.4	-772.0	-664.7
prior	0.25	0.25	0.25	0.25	0.25	0.25	0.25	0.25
likelihood	4.93×10^{-47}	$1.18\times 10^{+34}$	1.48×10^{-16}	$4.77\times 10^{+39}$	1.93×10^{-51}	$5.54\times 10^{+23}$	2.37×10^{-16}	$9.65\times 10^{+30}$
φ	1.03×10^{-86}	2.47×10^{-6}	3.09×10^{-56}	1.00	4.04×10^{-91}	1.16×10^{-91}	4.96×10^{-56}	2.02×10^{-9}

(b)

It was found that the effective connectivity between $M1_{left}$ and $M1_{right}$ can be explained by a bilinear connectivity model (Model 4), which is averagely preferred by the five subjects, as shown by Figure 7. $M1_{left}$ and $M1_{right}$ are effectively and bidirectionally connected to each other during bimanual tapping of hand fingers with the right and bimanual tapping of hand fingers as the input for $M1_{left}$ and the left and bimanual tapping of hand fingers as the input for $M1_{right}$. The $M1_{left} - M1_{right}$ connection is influenced by the modulatory input of the left hand while the $M1_{right} - M1_{left}$ connection is influenced by the modulatory input of the right hand. These connectivities are however not gated (influenced) by any of the two M1s, ruling out the possibility of the non-linear behavior of connections between both M1s. The average values of the DCM parameters that influence the between-region connections (a), the modulation of between-region connections (b) and the stimulus bound perturbation input (c) are shown in Figure 7 and tabulated in Table 4.
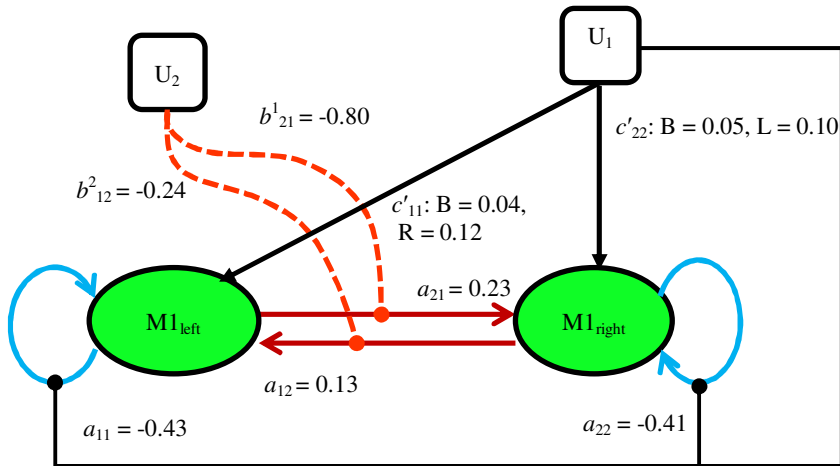
Figure 7: Bilinear effective connectivity model (Model 4) that has the best balance between fit/accuracy and complexity in explaining the bilateral tapping of hand fingers

TABLE 4: DCM Parameters that influence between-region connections (a), modulation of between-region connections (b) and the stimulus bound perturbation input (c). All values are in Hz (s^{-1}). The probability of each connection or modulation to occur is given in the brackets

	a_{11}	a_{12}	a_{21}	a_{22}	b^2_{11}	b^2_{12}	b^1_{21}	b^2_{22}	c_{11}	c_{12}	c_{13}	c_{21}	c_{22}	c_{23}
Subject 1	-0.60 (1.00)	0.10 (0.74)	0.07 (0.67)	-0.72 (1.00)	0	-0.14 (0.66)	-0.44 (0.87)	0	0.17 (1.00)	0	0.12 (0.98)	0	0.17 (1.00)	0.14 (0.99)
Subject 2	-0.47 (1.00)	0.12 (0.90)	0.35 (0.94)	-0.83 (1.00)	0	-0.70 (0.87)	-1.81 (0.99)	0	0.16 (1.00)	0	0.05 (0.91)	0	0.23 (1.00)	0.06 (0.80)
Subject 3	-0.81 (1.00)	0.44 (0.99)	0.24 (0.97)	-0.75 (1.00)	0	-0.89 (0.98)	-0.80 (0.85)	0	0.20 (1.00)	0	0.06 (0.84)	0	0.30 (1.00)	0.16 (0.98)
Subject 4	-0.96 (1.00)	0.21 (0.75)	-0.15 (0.71)	-0.87 (1.00)	0	-1.20 (0.94)	-1.58 (0.87)	0	0.20 (0.99)	0	0.17 (0.93)	0	0.22 (1.00)	0.17 (0.94)
Subject 5	-0.59 (1.00)	0.17 (0.94)	0.43 (0.96)	-0.71 (1.00)	0	0.10 (0.69)	-1.23 (0.98)	0	0.16 (1.00)	0	0.08 (0.98)	0	0.11 (1.00)	0.06 (0.85)
Average BMS	-0.43 (1.00)	0.12 (0.71)	0.23 (1.00)	-0.41 (1.00)	0	-0.24 (0.88)	-0.80 (0.99)	0	0.12 (0.99)	0	0.05 (1.00)	0	0.10 (1.00)	0.04 (1.00)

a_{11} = self connectivity on region 1 (M1$_{left}$), a_{22} = self connectivity on region 2 (M1$_{right}$)
a_{12} = connectivity from region 2 to region 1, a_{21} = connectivity from region 1 to region 2
b_{21} = induced connectivity on a$_{21}$ connection, b_{12} = induced connectivity on a$_{12}$ connection
c_{11} = input due to unilateral right hand tapping, c_{22} = input due to unilateral left hand tapping
c_{13} = input due to bilateral (left) hand tapping, c_{23} = input due to bilateral (right) hand tapping

4. DISCUSSION

4.1 Modelling the brain activation

In the first part of this study, the response variables in the primary motor cortices due to the left, right and bilateral finger tapping were observed for Y_j measurements with $j = 1$ to J (in step of 1), indexes the measurements. For each Y measurement, a set of $L(L < J)$ explanatory variables, denoted by x_{jl} were obtained with $l = 1$ to L (in step of 1), indexes the explanatory variables (Kiebel and Holmes (2004)). Thus, a general linear model that explains the response variable Y_j in the primary motor cortices, in terms of a linear combination of the explanatory variables x_{jl} and an error term (ε) can be written as (Kiebel and Holmes (2004)).

$$Y_j = x_{j1}\beta_1 + \cdots + x_{jl}\beta_l + \cdots + x_{jL}\beta_L + \varepsilon_j. \tag{1}$$

β_l is the unknown parameter corresponding to each of the L explanatory variables x_{jl}. The errors ε_j are normally-distributed random variables with the mean μ and variance σ^2 and can be written as $\varepsilon_j \sim N(\mu, \sigma^2)$ (Gelman *et al.* (2008)). It is also assumed that ε_j is independently and identically distributed (i.i.d) with $\mu = 0$. For the brain activations shown in Figure 3 (a – c) that incorporate the response variables for the right, left and bilateral tapping of the hand fingers, the general linear model for each measurement $j = 1$ to J and for β_l with $l = 1$ to 10 can be written in full as

$$Y_1 = x_{11}\beta_1 + x_{12}\beta_2 + \cdots + x_{110}\beta_{10} + \varepsilon_1$$
$$.$$
$$.$$
$$.$$
$$Y_j = x_{j1}\beta_1 + x_{j2}\beta_2 + \cdots + x_{j10}\beta_{10} + \varepsilon_2 \tag{2}$$
$$.$$
$$.$$
$$.$$
$$Y_J = x_{J1}\beta_1 + x_{J2}\beta_2 + \cdots + x_{J10}\beta_{10} + \varepsilon_j.$$

In Equation (2), the unknown parameters β_1, β_2 and β_3 correspond namely to the explanatory variables for the left, right and bilateral tapping of hand fingers while $\beta_4 - \beta_9$ model any movement related effects that occurs during the scan. β_{10} is the unknown that represents the baseline responses that occurs in the brain during the fMRI experiment. It can be seen from Equation (2) that Y is the measured time series data of length J and can represent any given voxel in the brain. Equation (2) can be written in matrix form of

$$
\begin{bmatrix} Y_1 \\ \cdot \\ \cdot \\ \cdot \\ \cdot \\ \cdot \\ \cdot \\ Y_j \\ \cdot \\ \cdot \\ \cdot \\ \cdot \\ \cdot \\ Y_J \end{bmatrix}
=
\begin{bmatrix}
x_{11} & x_{12} & \cdots & \cdots & x_{10} \\
\cdot & \cdot & & & \cdot \\
\cdot & \cdot & & & \cdot \\
\cdot & \cdot & & & \cdot \\
\cdot & \cdot & & & \cdot \\
\cdot & \cdot & & & \cdot \\
x_{j1} & x_{j2} & \cdots & \cdots & x_{j10} \\
\cdot & \cdot & & & \cdot \\
\cdot & \cdot & & & \cdot \\
\cdot & \cdot & & & \cdot \\
\cdot & \cdot & & & \cdot \\
x_{J1} & x_{J2} & \cdots & \cdots & x_{J10}
\end{bmatrix}
\begin{bmatrix} \beta_1 \\ \beta_2 \\ \beta_3 \\ \beta_4 \\ \beta_5 \\ \beta_6 \\ \beta_7 \\ \beta_8 \\ \beta_9 \\ \beta_{10} \end{bmatrix}
+
\begin{bmatrix} \varepsilon_1 \\ \cdot \\ \cdot \\ \cdot \\ \cdot \\ \cdot \\ \varepsilon_j \\ \cdot \\ \cdot \\ \cdot \\ \cdot \\ \cdot \\ \varepsilon_J \end{bmatrix}.
\tag{3}
$$

Equation (3) in matrix notation is then

$$ Y = X\beta + \varepsilon. \tag{4} $$

In Equation (4), Y represents the column vector of observations, ε the column vector of error terms and β is the column vector of the unknowns, i.e. β_1 to β_{10}. X is known as the design matrix of dimension $(J,10)$. In rows, it is a combination of the general linear models that represent the observations, while in columns it contains the explanatory variables which contains all the effects that influence the measured signal such as the signals from the unilateral and bilateral tapping of hand fingers or other effects such as subject's translational and rotational movements.

The design matrix for a single subject is depicted in Figure 8(a) while Figure 8(b) is the design matrix for the seven subjects.

Given Y and X, the unknown parameters β_1 to β_{10} can be estimated using the least square fitting method (Kiebel and Holmes (2004)) to look for any effect such as the difference between active and rest states or the difference in the effects between any two conditions. In doing that, a statistic for each brain voxel that tests for the effect of interest in that voxel is calculated, resulting in a large volume of statistic for the whole brain volume.

One now has to decide whether this volume shows any evidence of the effect. To achieve this, an independent *t*-test is conducted between data collected during the active and rest states or between any two conditions of interest and the *t* values obtained is compared to the null distribution for the *t* statistic.

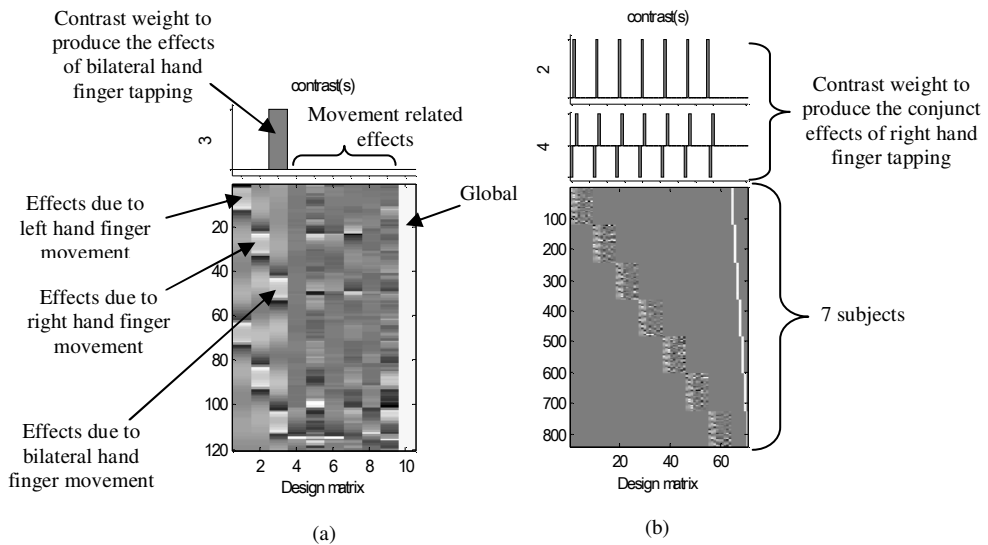

Figure 8: Design matrix for (a) single subject and (b) multiple subject FFX analysis

In this study, the *t* value for each time series voxel for the *T*-contrast images shown in Figures 3(a) – (c) is calculated from the relation (Poline *et al.* (2004))

$$t = [c^T\beta]/[\sqrt{\mathrm{var}[c^T\beta]}].\tag{5}$$

Equation (5) can also be written as (Poline *et al.* (2004))

$$t = \left[c^T \beta \right] \Big/ \left[\sigma \left(c^T \left(X^T X \right)^{-1} c \right)^{1/2} \right] \qquad (6)$$

from which c is the weight of the parameter estimates used to form the numerator of the statistics, c^T is the transposed matrix of c, β is the parameter of the model to be estimated (i.e. $\beta_1 - \beta_{10}$), σ is the standard deviation and X and X^T is the designed matrix and its transposition respectively. The parameter c is actually a vector or matrix that contains the contrasts weights. In other words, the t value is the contrast of the estimated parameters or the effect size, $c^T \beta$, divided by the square root of the variance estimate which is $\text{var}\left[c^T \beta \right]$. The contrast weights must be specified to define the contrast. For example, in Figure 8(a), the contrast weight is taken as [0 0 1 0 0 0 0 0 0] in order to obtain the effects due to bilateral tapping of a single subject. The effect size is basically obtained from the comparison between the effects of bilateral tapping with baseline. In Figure 8(b), a slightly different contrast weight (i.e. [-1 0 1 0 0 0 0 0 0 0] conjunct with [0 1 0 0 0 0 0 0 0 0]) is implemented on multiple subjects design matrix to obtain the conjunction of the effects of the right unilateral tapping with the effects of bilateral tapping minus the left unilateral tapping.

This is done to obtain the brain area that specifically controls the tapping of the right hand fingers during both unilateral right and bilateral tapping. Conjunction analysis of this type permits not only the determination of the areas in the brain for a specific function that are common in all subjects under study, it also allows the identification of areas that share a specific function in a subject.

The colored regions or blobs on the statistical parametric maps (shown in Figures 3(a) – (c)), hence, represent the statistical image of the effects of interest, for example the activated brain areas during the taping of the left, right and bilateral fingers.

The results are obtained from the application of t-test (T contrast) on each voxel and by taking the p value smaller than a designated alpha (α) value as significant. In other words, for a given voxel, the general linear model, by means of least square fitting, will figure out just what type that voxel is by modelling it as a linear combination of the hypothetical time series as discussed earlier (Kiebel & Holmes (2004)). The fitting or estimation entails finding the parameter values ($\beta_1 - \beta_{10}$) such that the linear combination best fits the measured data.

4.2 Functional specialization and response change

Based on Figures 3 (a – c) and Figures 4 (a – d), it is quite interesting to see that $M1_{right}$ (the control of the left hand finger tapping) shows a larger number of activated voxels but with a relatively lower activation response as compared to $M1_{left}$ (the control of the right-hand finger tapping), as opposed to our previous study (Ahmad Nazlim Yusoff et $al.$ (2010a, 2010b, 2010c)) on multiple subjects performing self-paced tapping of hand fingers, despite the fact that all the subjects in the present and previous studies were right handed. This suggests that the spatial and height extent of activation may differ between externally triggered and self-paced tapping of hand fingers.

In our previous study (Ahmad Nazlim Yusoff et $al.$ (2010a, 2011)), we found that the average activation area is larger in $M1_{left}$ during unilateral right hand finger tapping as compared to $M1_{right}$ during unilateral left hand finger tapping. The study used a robust self-paced finger tapping. Prior to the fMRI scan, the subjects were told that they need to tap their fingers two times in one second using an intermediate force between too soft and too hard. However, since all the subjects were right-handed, there would be a tendency for the subjects to tap their preferred hand fingers faster than their non-preferred hand fingers, resulting in the rate effects that will cause higher activation in terms of number of activated voxel. It has been reported that the rate effects will cause higher activation both in terms of signal intensity and number of activated voxel (Jäncke et $al.$ (1998)). In the present study, the rate effects did not come into play since the tapping is externally triggered at a constant pace. The findings obtained from this study are however in good agreement with a multiple subject fMRI study on unilateral and bilateral sequential movement in right-handers (Jäncke et $al.$ (1998) and Lutz et $al.$ (2005)). The authors reported that the right hemisphere showed more activation than the left hemisphere in both unilateral and bilateral task at two tapping frequencies. Their interpretations are that right-handers expend more effort to perform with their non-preferred hand. A stronger

activation pattern in the right hemisphere is the result of trying to perform the tapping task using a system that is slightly less competent with the implication that the more skilled and competent system will expend less effort and will therefore provide a relatively weaker activation. Based on the interpretation given above, it seemed that the influence of the average effects of the sub-dominant hand is greater than the effects that would be produced by the dominant hand.

Interestingly, in contrast to the spatial extent of activation, the change in response for M1 obtained in this study is relatively higher in $M1_{left}$ (during the right hand finger tapping) as compared to the change in response measured in $M1_{right}$ (during the left hand finger tapping) see Figures 4(a) and (b). This finding is in contrast to the number of activated voxels which is higher for the tapping of the left hand fingers as compared to tapping of the right hand fingers. In relation to the discussion above, it can be assumed that if the tapping pace is kept constant (using an external trigger) hand dominancy does not influence the height extent of activation as it does on the spatial extent of activation. As a result, the higher change in response observed in $M1_{left}$ is potentially due only to the tendency of these right-handers to press their fingers harder against the thumb using their dominant hand fingers, whereby a larger force will activate a higher response. In an fMRI study on ten right handed subjects that were instructed to squeeze the sphygmomanometer rubber bulb at different pressure level (Thickbroom *et al.* (1998)) using finger flexion of their dominant hand, an increase in response in terms of signal intensity, signal density and even voxel count have been demonstrated as the pressure level (force) is increased. The finding in our study is also supported by another fMRI study on brain activation during precision and power gripping by Kuhtz-Buschbeck *et al.* (2008) that has revealed a positive linear relationship between the blood oxygenation level dependent (BOLD) signal intensity in the left M1 and right cerebellum with the grip force. They have also managed to show in their communication, a number of published coordinates of brain regions with force-related increases in brain activity (activation) that have been obtained by many studies before. Interestingly, there are also other studies that discover negative relationship between the force and brain activation (i.e. deactivation) see for example Ward and Frackowiak (2003). However, the number is superseded by the studies that show brain activation increase as the force is increased.

For bilateral tapping of hand fingers, the number of activated voxels in $M1_{left}$ and $M1_{right}$ and their responses are about the same. This behavior has also been found in our previous study (Ahmad Nazlim Yusoff *et al.* (2011)) on self-paced tapping of hand fingers. A neural network study on bilateral hand movement conducted by Walsh *et al.* (2008) using structural equation modeling (SEM) indicated that the activation during bilateral hand movement is not supposed to be equal to the addition of the activation obtained from unilateral left and right hand finger movements. They have also found that the intra hemispheric connectivity network within each hemisphere was found to be different during unilateral tapping.

However, the connectivity network in one hemisphere is a mirror image of the network in the other hemisphere during bilateral tapping. It has also been previously suggested (Serrien *et al.* (2003)) that the increase in the interaction between sensory motor cortices in both hemisphere is required for bilateral hand movement from which the activity in the non dominant hemisphere is driven by the activity in the dominant hemisphere (Walsh *et al.* (2008)). Another compelling study was by Grefkes *et al.* (2008) which used DCM to investigate the cortical network during unilateral and bilateral hand movements. They reported that during bilateral hand movement, there will be an increase in the intra hemispheric connectivity and transcallosal coupling of the supplementary motor area (SMA) and M1 which in turn mediates the facilitation of neural activity, associated with bilateral hand movement. Thus, it can be said that during bilateral tapping of hand fingers, the average effects in both the $M1_{left}$ and $M1_{right}$ seemed to be contributed by the simultaneous control of both the left and right hand finger tapping. In performing the tapping, all the subjects have two common objectives which are 1) to tap their fingers according to the external trigger and 2) to perform a simultaneous and in-phased tapping of the left and right hand fingers. Such coordination, according to the previous studies mentioned previously, will generate a symbiotic network effect between the dominant and non dominant hemispheres, from which the dominant hemisphere will drive the activation in the non dominant hemisphere resulting in an equal spatial (area) and height (intensity) extent of activation in both $M1_{left}$ and $M1_{right}$.

In relation to the discussion above, it is quite interesting to conclude the mutual dependency between $M1_{left}$ and $M1_{right}$ during bilateral tapping of hand fingers in the perspective of regression analysis results given in Figure 5(a) and (b). The results obtained from regression analysis represent, among others, the temporal correlation between two activated areas, hence functional connectivity. It can be clearly seen that the relative response in $M1_{left}$ and $M1_{right}$ during bilateral tapping fulfilled a good, positive, linear

and significant relationship with each other and in accordance with the existence of a symbiotic network effect as mentioned in the previous paragraph. The increase in the relative response in one region will cause an increase in the other. However, the study of functional connectivity is limited by the regression model itself and is not mechanistic in nature and would not be able to conclude on the causal nature of the activation in $M1_{left}$ and $M1_{right}$. In order for the cause-effects relationship to be studied, DCM is implemented on the present fMRI data and will be discussed in detail in the next section.

The results shown in Figure 3 (d) and (e) reveal another interesting behavior of brain activation in this study. The activations were obtained by subtracting the effects of a unilateral tapping from the effects of bilateral tapping, conjunct with the effects of the other unilateral tapping. The resultant of this conjunction of contrasts is an accentuation of the same particular area in the brain that involved in the tapping of the left or right hand fingers during both the unilateral and bilateral taping. An example of the design matrix used for this conjunction of contrast is shown in Figure 8(b) from which the same area in the brain involved in controlling both the unilateral and bilateral tapping of right hand fingers can be made visible. As can be seen in Figure 3(d) and (e), the intriguing question is why does the activation in the right hemisphere is very much smaller than the activation in the left hemisphere. One logical basis that can potentially be the answer to the question appears to be in the fact that all subjects are right hand dominant. It is suggested that, for right handed individuals, the same larger motor area is recruited to be involved in performing the unilateral as well as the bilateral tapping using the dominant hand as compared to the non dominant hand from which the same smaller area is involved in both the unilateral and bilateral tapping. However, a continuation of this study onto a group of left handed subjects is necessary in order for a more accurate interpretation of the results obtained in the present study.

4.3 The dynamic causal model and the effective connectivity

In the second part of this study, we investigated the effective connectivity between the two primary motor areas, primarily the $M1_{left}$ and $M1_{right}$, using the dynamic causal modeling (DCM). The justifications of these two regions being selected were because they are significantly activated at corrected p value (Figure 3) and their well known involvement in controlling the tapping of the right and left hand fingers (Grefkes *et al.* (2008); Walsh *et al.* (2008); Ahmad Nazlim Yusoff *et al.* (2010a, 2011)).

DCM uses a fully Bayesian approach i.e. Bayesian model selection (BMS), in comparing the linear, bilinear and non-linear models shown in Figure 1 and in selecting the most optimum model among the competing models. BMS is fully statistic in approach and computes an approximation to the model evidence $p(y|m)$, which is the probability of obtaining the data y, given the model m (Stephan *et al.* (2009)). It quantifies the properties of a good model by explaining the data as accurately as possible and has minimal complexity. All the eight models were compared by optimising the probability of conditional density for each model, given its respective log-evidence. In another words, BMS determines the model which provides the best balance between fit/accuracy and complexity given the fMRI data.

The fact that bilinear models family has been chosen in BMS analysis (see Figure 6) indicates that the probable cortical network during bilateral tapping of hand fingers is neither falls into group of models with quite a simple and straight forward kind of network as suggested by Model 1 and 2, nor it is from a much more complicated group of models with non linear connectivity between regions as represented by Model 5 to 8. The optimum model rather falls in between the two extremes with connectivity among the two regions being influenced by experimental modulation.

The most optimal model among the eight competing models was finally chosen. The results obtained from BMS for both group RFX and FFX analyses are in good agreement for Model 4, see Table 3. The lowest value of the sum of negative free energy (ΣF) in both the FFX and RFX perspectives indicates that the best balance between accuracy and complexity has been met by Model 4. Thermodynamically, the free energy (F) is the difference between the energy of a system (E) and its entropy (S) (Friston (2010)), or

$$F = E - S. \tag{7}$$

Analogously, in brain network modeling, E is simply the log-evidence or log $p(y|m)$ of a model. In Friston (2010) it is defined as the surprise (or self information) about the joint occurrence of sensory input and its causes (or unknown parameters, ϑ). According to Stephan *et al.* (2009), S can be represented by Kullback-Leibler (KL) divergence between the approximating posterior density of the unknown parameters, $q(\vartheta)$ and the true posterior distribution, $p(\vartheta|y,m)$. Equation (7) can thus be written as

$$F = \log p(y|m) - KL[q(\vartheta), p(\vartheta|y, m)] \qquad (8)$$

or

$$F = \langle \log p(y|\vartheta, m) \rangle_q - KL[q(\vartheta), p(\vartheta|m)] \qquad (9)$$

if approximation is made onto the conditional density of Equation (8).

In Equation (9), accuracy is the first term on the right side of the equation which explains the probability of obtaining observed data y given a particular model m with parameters ϑ, while complexity is reflected in the second term which contains the amount of information that can be obtained from the data with regards to the parameters of a model, see Stephan *et al.* (2009). The smallest difference between accuracy and complexity exhibited by Model 4 has the meaning that F is minimised in such a way that the model parameters has been fitted well, from which the fitted data behave as close as possible to the observed experimental data despite the complexity of the model.

The Dirichlet parameter estimates, α_d, the expected posterior probability, r and the exceedance probability, ψ depicted in Table 3 are all the parameters used in BMS analyses to rank models at group RFX level. The Dirichlet parameter estimates is a measure of effective number of subjects in which a given model generated the observed data. The sum of all α_d is equal to the number of subjects plus the number of compared models which is 13 in this study. With $\alpha_d = 5.0640 \approx 5$ for Model 4, it can be said that the model has been agreed upon by all the five subjects. The exceedance probability ψ is the probability that a given model is more likely than any other model to give the observed experimental data. If ψ obtained for Model 4 from 8 models is 0.92 (or 92%), we can be 92% sure that the favoured model has a greater posterior probability ($r = 0.67$) than any other tested models. As can be seen in Table 3(a), the sum of ψ for all models is unity. The histograms in Figure 6(b) graphically indicate the expected posterior probability and the exceedance probability for all models. Both two quantities for Model 4 are comparatively higher than any other models. From Table 3(a), it can be concluded that all the values of α_d, ψ and r agree very well that the bilateral tapping is best represented by Model 4. Furthermore, these model has also shown firm evidence in FFX perspective with a high posterior model probability ($\varphi = 1.0000$) in getting the respective log-evidence (or likelihood $= 4.77 \times 10^{39}$), see Table 3(b) and Figure 6 (top).

In view of the model structure used in this study that is assumed to be identical across subjects (Stephan *et al.* (2010)), the results obtained from RFX for BMS is more reliable. More importantly, the results obtained from group BMS studies whether in RFX or FFX perspectives, have been reported (Stephan *et al.* (2010)) to be able to take into consideration the presence of outliers that could have arisen in any subject under study.

This study has been able to fit the effective connectivity between $M1_{left}$ and $M1_{right}$ with a bilinear model, see Figure 7. Thus, the null hypothesis that no single model is better than any other model is rejected. The effective connectivity is a dynamic quantity. It defines the influence within a physical system, i.e. the brain at cortical level, in response to the external manipulations or inputs. The effective connectivity between $M1_{left}$ and $M1_{right}$ shown in Figure 7 is driven by a stimulus-bound perturbation input (U_1). The source of these input is the coordination and control of bilateral tapping of hand fingers by the primary motor region, denoted by (B) in the figure. Included in the model as U_1 as well is the underlying exclusive and respective control of the left and right hand finger tapping that is thought to come into play, intrinsically, during the bilateral tapping, and are denoted by (L) or (R). Thus, it can be said that, the effective connectivity between $M1_{left}$ and $M1_{right}$ that took place during bilateral tapping is bidirectional in nature and is caused by unilateral and bilateral control of hand fingers by the subjects. Nevertheless, the effective connectivity between the two regions was found to be not only initiated by the direct input but was also influenced by modulatory input (U_2), originating from the attentional movement in order for the tapping to be performed simultaneously and in-phase between the left and right hand fingers. This attentional movement is also assigned to the exclusive and respective control of the left and right hand finger tapping. In addition, the stimulus-bound peturbation input modulates the self connectivity in each region to impose saturation-like effects (Friston *et al.* (2003)). The effective connectivity between $M1_{left}$ and $M1_{right}$ however, is not gated (influenced) by any of the two M1s, ruling out the possibility of non-linear behavior of connections between $M1_{left}$ and $M1_{right}$ as indicated by Model 5 - Model 8 in Figure 1.

The DCM parameter values shown in Figure 7 are obtained from Bayesian parameter averaging (BPA) computation from which the values are shown in Table 4 together with the values for individual subject and the definition for various DCM parameters. The effective connectivity from $M1_{left}$ to $M1_{right}$ was found to be larger than from $M1_{left}$ to $M1_{right}$ indicating a higher transfer rate of signal from the left to right hemisphere as compared to the contra direction during bilateral tapping. Despite the fact that bilateral

tapping induced equal change in signal intensity and spatial extent of activation in $M1_{left}$ and $M1_{right}$ as stated in an earlier discussion, the two quantities can be understood as the result of the underlying network mechanism that has occurred. For a right handed subject performing bilateral hand movement, the dominant hemisphere is the left hemisphere. According to Serrien *et al.* (2003) and Walsh *et al.* (2008), an increase in the interaction between motor cortices from the two hemispheres is observed during bilateral hand movement from which the dominant hemisphere will drive the non dominant side causing the effective connectivity to be higher from left hemisphere to right hemisphere as compared to the connectivity in the opposite direction.

It is also evident from Figure 7 and Table 4 that the strength of the driving inputs that drive the activity and modulate the self connection in both the $M1_{left}$ and $M1_{right}$ regions are about the same. As mentioned earlier, in performing the bilateral tapping, the subjects will have to coordinate their fingers so that the tapping of both hands will be in-phase and according to the external trigger. These two similar objectives that need to be fulfilled by the subjects will certainly induce similar driving input into the $M1_{left}$ and $M1_{right}$ regions which in turn equally modulate self connection in $M1_{left}$ and $M1_{right}$.

As discussed above, the effective connectivity between $M1_{left}$ and $M1_{right}$ is influenced by the modulatory input, U_2. A stronger modulatory input is needed to modulate the effective connectivity of a higher strength as indicated in Figure 7. The negative values of the effects of modulatory input on $M1_{left} \rightarrow M1_{right}$ and $M1_{right} \rightarrow M1_{left}$ connections were due to the fact that modulation on the connection reduces the influence that one region has on another.

4.4 The dynamic causal model for bilateral finger tapping: a mathematical formulation

Finally, given an optimum causal model that would be able to explain the network mechanism in the brain during bilateral tapping of hand fingers, it is also very important to mathematically understand the exact mechanism within any one brain region used to construct the network and how the activity within one brain region is influenced by experimental manipulations. To achieve this, a minor modification is made onto the dynamic causal model shown in Figure 7 and is given in Figure 9.

While U_1 and U_2 are exclusively defined as the driving and modulatory inputs in Figure 7, in Figure 9 they are the similar inputs that drive the activity in $M1_{left}$ and $M1_{right}$ and modulate their intrinsic and self connections. The modification made however, did not change the structure of the models and their biophysical concept that has been used in DCM analysis but remains the same as described in the method section. The model shown in Figure 9 was also constructed based on the bilinear state equation in the form of (Friston *et al.* (2003))

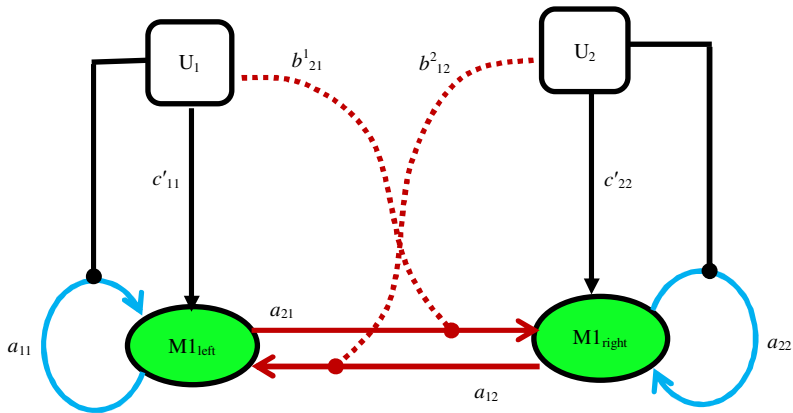$$\dot{x} = \left(A + \sum_{i=1}^{m} u_i B^{(i)} \right) x + Cu. \tag{11}$$

Figure 9: Modified bilinear effective connectivity model as explained in the text

In Equation (11), A is the matrix that represents the fixed or context-independent strength of connections between the modelled regions (intrinsic couplings) and the matrices B^j represent the modulation of these connections. The matrix C is free of x but its role is to model the extrinsic influences of inputs on neuronal activity. In the absence of input u, the time dependent, $\dot{x} = Ax$, which implies that the only existing connectivities are that of the intrinsic couplings between the regions of interest (ROIs). Due to the linear dependency between $\dot{x}$ and xu, the model is called bilinear model (Penny *et al.* (2004)).

Based on Figure 9, Equation (11) can then be expanded into

$$
\begin{aligned}
\begin{bmatrix} \dot{x}_1 \\ \dot{x}_2 \end{bmatrix} &= \left(\begin{bmatrix} a_{11} & a_{12} \\ a_{21} & a_{22} \end{bmatrix} + u_1 \begin{bmatrix} 0 & 0 \\ b_{21}^{~1} & 0 \end{bmatrix} + u_2 \begin{bmatrix} 0 & b_{12}^{~2} \\ 0 & 0 \end{bmatrix} \right) \begin{bmatrix} x_1 \\ x_2 \end{bmatrix} \\
&\quad + \begin{bmatrix} c'_{11} & 0 \\ 0 & c'_{22} \end{bmatrix} \begin{bmatrix} u_1 \\ u_2 \end{bmatrix} \\
&= \begin{bmatrix} a_{11} & a_{12} \\ a_{21} & a_{22} \end{bmatrix} \begin{bmatrix} x_1 \\ x_2 \end{bmatrix} + u_1 \begin{bmatrix} 0 & 0 \\ b_{21}^{~1} & 0 \end{bmatrix} \begin{bmatrix} x_1 \\ x_2 \end{bmatrix} + u_2 \begin{bmatrix} 0 & b_{12}^{~2} \\ 0 & 0 \end{bmatrix} \begin{bmatrix} x_1 \\ x_2 \end{bmatrix} \\
&\quad + \begin{bmatrix} c'_{11} & 0 \\ 0 & c'_{22} \end{bmatrix} \begin{bmatrix} u_1 \\ u_2 \end{bmatrix}
\end{aligned}
\tag{12}
$$

with $\dot{x}_1$ is the activity in M1$_{\text{left}}$ and $\dot{x}_2$ is the activity in M1$_{\text{right}}$. The rest of the matrix elements in Equation (12) are defined in Table 4. Note that in Figure 9 and Equation (12), $c'_{11} = c_{11} + c_{23}$ while $c'_{22} = c_{22} + c_{13}$. With the presence of intrinsic coupling and its modulation, the change in neuronal activity in terms of linearly separable components that reflect the influence of other state variables can be formulated. Thus, the activity in M1$_{\text{left}}$ ($\dot{x}_1$) and M1$_{\text{right}}$ ($\dot{x}_2$) can be written as

$$
\dot{x}_1 = a_{11}x_1 + a_{12}x_2 + b_{12}^{~2}x_2 u_2 + c'_{11}u_1
$$

$$
\dot{x}_2 = a_{22}x_2 + a_{21}x_1 + b_{21}^{~1}x_1 u_1 + c'_{22}u_2.
\tag{13}
$$

Substituting Equation (13) with the average values obtained from DCM (see Figure 9 and Table 4), the activity in M1$_{\text{left}}$ and M1$_{\text{right}}$ regions can be represented by

$$
\dot{x}_1 = 0.43x_1 + 0.13x_2 - 0.24x_2 u_2 + 0.16u_1
$$

$$
\dot{x}_2 = -0.41x_2 + 0.23x_1 - 0.80x_1 u_1 + 0.15u_2
\tag{14}
$$

Equation (14) provides, in mathematical form of what has been discussed earlier. It simply expresses that the activity in M1$_{\text{left}}$ is a function of time and is not exclusive but very much dependent on what is happening in M1$_{\text{right}}$. The same goes to M1$_{\text{left}}$ which has some influence on the activity

in $M1_{right}$. The two regions are driven by the stimulus-bound perturbation input and from there on executed connectivity that are influenced by the modulatory input. The modulation on connection has an effect of reducing the influence one region has on another, rendering the values negative. The driving input also has some influence on modulating the self connection in each particular region.

5. CONCLUSION

In conclusion, this study has been able to fit the observed fMRI data acquired from bilateral tapping of hand fingers performed by right handed subjects to a general linear model for brain activation and to a bilinear dynamic causal model for the effective connectivity between $M1_{left}$ and $M1_{right}$ regions. The findings obtained from the analysis of brain activation correlated well with that of effective connectivity from which it has been determined that the dominant hemisphere which is the left hemisphere has some influence in promoting the activation in the non dominant hemisphere during bilateral finger tapping. The effective connectivities between $M1_{left}$ and $M1_{right}$ were not only driven by the coordination and control of bilateral tapping of hand fingers by the primary motor region but were also influenced by the attentional movement of fingers in both hands in order for the tapping to be performed simultaneously, in-phase and following the external trigger. Thus, the null hypothesis that no single model is better than any other model is rejected. This study has revealed important fundamental information for future fMRI studies on motor coordination and is viable to be implemented in clinical environment. However, due to the different approaches used in the study of hand finger movement employing various tasks and methods, we found that it is quite difficult for a direct comparison with the results obtained from other studies to be made.

ACKNOWLEDGEMENT

REFERENCES

Ahmad Nazlim Yusoff, Aini Ismafairus Abd Hamid, Khairiah Abdul Hamid, Wan Ahmad Kamil Wan Abdullah, Mazlyfarina Mohamad. 2011. Functional specialization and effective connectivity during self-paced unimanual and bimanual tapping of hand fingers: An extended analysis using dynamic causal modeling and Bayesian model selection for group studies. *Malaysian Medical and Health Science Journal*. **7**(2): 17 - 36.

Ahmad Nazlim Yusoff, Mazlyfarina Mohamad, Aini Ismafairus Abd Hamid, Wan Ahmad Kamil Wan Abdullah, Mohd Harith Hashim and Nurul Zafirah Zulkifli. 2010a. Functional specialization and effective connectivity in cerebral motor cortices: An fMRI study on seven right handed female subjects. *Malaysian Journal of Medicine and Health Sciences.* **6**(2): 71 - 92.

Ahmad Nazlim Yusoff, Mazlyfarina Mohamad, Khairiah Abdul Hamid, Aini Ismafairus Abd Hamid, Hanani Abdul Manan and Mohd Harith Hashim. 2010b. Intrinsic couplings between the primary motor area (M1) and supplementary motor area (SMA) during unilateral finger tapping task. *Akademi Sains Malaysia Journal of Science.* **4**(2): 158 - 172.

Ahmad Nazlim Yusoff, Mazlyfarina Mohamad, Khairiah Abdul Hamid, Aini Ismafairus Abd Hamid, Hanani Abdul Manan and Mohd Harith Hashim. 2010c. Activation characteristics of the primary motor (M1) and supplementary motor (SMA) areas during robust unilateral finger tapping task. *Malaysian Journal of Health Sciences.* **8**(2): 43 - 49.

Aini Ismafairus Abd Hamid, Ahmad Nazlim Yusoff, Siti Zamratol-Mai Sarah Mukari, Khairiah Abdul Hamid, Mazlyfarina Mohamad and Hanani Abdul Manan. 2011. Brain activation during addition and subtraction task in noise and in quiet. *Malaysian Journal of Medical Sciences*. **18**(3): 3 - 15.

Büchel, C. and Friston, K. 2000. Assesing interactions among neuronal systems using functional neuroimaging. *Neural Networks.* **13**: 871 - 882.

Eickhoff, S. B., Stephan, K. E., Mohlberg, H., Grefkes, C., Fink, G. R., Amunts, K. and Zilles, K. 2005. A new SPM toolbox for combining probabilistic cytoarchitectonic maps and functional imaging data. *Neuroimage.* **25**: 1325 - 1335.

Friston, K. J. 2005. Models of brain function in neuroimaging. *Annual Review in Psychology.* **56**: 57 - 87.

Friston, K. J. 2010. The free energy principle: a rough guide to the brain? *Trends in Cognitive Sciences.* **13**(7): 293 - 301.

Friston, K. J., Harrison, L. and Penny, W. 2003. Dynamic causal modeling. *Neuroimage.* **19**: 1273 - 1302.

Friston, K. J., Holmes, A. Poline, J. B., Price, C. J. and Frith, C. D. 1996. Detecting activations in PET and fMRI: Levels of inference and power. *Neuroimage.* **40**: 223 - 235.

Gelman, A., Carlin, J. B., Stern, H. S. and Rubin, D. B. 2004. *Bayesian Data Analysis,* 2nd Ed. Boca Raton: Chapman and Hall/CRC.

Grefkes, C., Eickhoff, S. B., Nowak, D. A., Dafotakis, M. and Fink, G. R. 2008. Dynamic intra- and interhemispheric interactions during unilateral and bilateral hand movements assessed with fMRI and DCM. *Neuroimage.* **41**: 1382 - 1394.

Jäncke, L., Peters, M., Schlaug, G., Posse, S., Steinmetz, H. and Müller-Gärtner, H. W. 1998. Differential magnetic resonance signal change in human sensori motor cortex to finger movements of different rate of the dominant and subdominant hand. *Cognitive Brain Research.* **6**: 279 - 284.

Kiebel, S. and Holmes, A. 2004. The general linear model. In Frackowiak, R.S.J., Friston, K. J., Price, C. J., Zeki, S., Ashburner, J. and Penny, W. D. (eds.) *Human brain function,* pp. 725 - 760. Elsevier Academic Press, Amsterdam.

Kuhtz-Buschbeck, J. P., Gilster, R., Wolff, S., Ulmer, S., Siebner, H. and Jansen, O. 2008. Brain activity is similar during precision and power gripping with light force: An fMRI study. *Neuroimage.* **40**: 1469 - 1481.

Lutz, K., Koeneke, S., Wüstenberg, T. and Jäncke, L. 2005. Asymmetry of cortical activation during maximum and convenient tapping speed. *Neuroscience Letter.* **373**: 61 - 66.

Nolte, J. 2009. *The human brain: An introduction to its functional anatomy* 6th Ed. Philadelphia: Mosby Elsevier.

Oldfield, R.C. 1971. The assessment and analysis of handedness: The Edinburgh Inventory. *Neuropsychologia.* **9**: 97 - 113.

Penny, W. D., Stephan, K. E., Mechelli, A. and Friston, K. J. 2004. Comparing dynamic causal models. *Neuroimage.* **22**: 1157 - 1172.

Poline, J. B., Kherif, F., and Penny, W. D. 2004. Contrast and classical inference. In Frackowiak, R.S.J., Friston, K. J., Price, C. J., Zeki, S., Ashburner, J. & Penny, W. D. (eds.) *Human brain function,* pp. 761 - 779. Elsevier Academic Press, Amsterdam.

Serrien, D. J., Cassidy, M. J. and Brown, P. 2003. The importance of the dominant hemisphere in the organisation of bimanual movements. *Human Brain Mapping.* **18**(4): 296 - 305.

Stephan, K. E., Kasper, L., Harrison, L. M., Daunizeau, J., den Ouden, H. E. M., Breakspear, M. and Friston, K. J. 2008. Nonlinear dynamic causal models for fMRI. *Neuroimage.* **42**: 649 - 662.

Stephan, K. E., Penny, W. D., Daunizeau, J., Moran, R. J. and Friston, K. J. 2009. Bayesian model selection for group studies. *Neuroimage.* **46**: 1004 - 1017.

Stephan, K. E., Penny, W. D., Moran R. J., den Ouden, H. E. M., Daunizeau, J. and Friston, K. J. 2010. Ten simple rules for dynamic causal modeling. *Neuroimage.* **49**: 3099 - 3109.

Thickbroom, G. W., Phillips, B. A., Morris, I., Byrnes, M. L. and Mastaglia, F. L. 1998. Isometric force-related activity in sensorimotor cortex measured with functional MRI. *Experimental Brain Research.* **121**: 59 - 64.

Walsh, R. R., Small, S. L., Chen, E. E. and Solodkin, A. 2008. Network acivation during bimanual movements in humans. *Neuroimage.* **43**: 540 - 553.

Ward, N. S. and Frackowiak, R. S. 2003. Age-related changes in the neural correlates of motor performance. *Brain.* **126**: 873 - 888.